Solar Wind Control of Magnetosheath Jet Formation and Propagation to the Magnetopause

Adrian T. LaMoury[1], Heli Hietala[1], Ferdinand Plaschke[2], Laura Vuorinen[3], and Jonathan P. Eastwood[1]

[1]The Blackett Laboratory, Imperial College London, London, UK
[2]Space Research Institute, Austrian Academy of Sciences, Graz, Austria
[3]Department of Physics and Astronomy, University of Turku, Turku, Finland

Key Points:

- THEMIS data from 2008–2018 are used to constrain conditions for jet formation and propagation to the magnetopause
- Jets reach the magnetopause 12x more often during low IMF cone angles and 5x more often during high solar wind speeds
- Low IMF magnitude, high Alfvén Mach no., and low density double expected impacts while dynamic pressure and plasma beta have no net effect

Corresponding author: Adrian LaMoury, adrian.lamoury15@imperial.ac.uk

Abstract

Magnetosheath jets are localized high-dynamic pressure pulses originating at Earth's bow shock and propagating earthward through the magnetosheath. Jets can influence magnetospheric dynamics upon impacting the magnetopause; however a significant fraction dissipate before reaching it. In this study we present a database of 13,096 jets observed by the Time History of Events and Macroscale Interactions during Substorms (THEMIS) spacecraft from 2008–2018, spanning a solar cycle. Each jet is associated with upstream solar wind conditions from OMNI. We statistically examine how solar wind conditions control the likelihood of jets forming at the shock, and the conditions favorable for jets to propagate through the magnetosheath and reach the magnetopause. We see that, for each solar wind quantity, these two effects are separate, but when combined, we find that jets are nearly 12 times more likely to reach and potentially impact the magnetopause when the interplanetary magnetic field (IMF) is at a low cone angle, and approximately 5 times more likely during fast solar wind. Low IMF magnitude, high Alfvén Mach number, and low density approximately double the number of jets at the magnetopause, while plasma beta and dynamic pressure display no net effect. Due to the strong dependence on wind speed, we infer that jet impact rates may be solar cycle dependent as well as vary during solar wind transients. This is an important step towards forecasting the space weather effects of magnetosheath jets, as it allows for predictions of jet impact rates based on measurements of the upstream solar wind.

Plain Language Summary

When the solar wind, a constant flow of plasma from the Sun, meets Earth's magnetic field, a shock wave forms in space. Like a rock in a stream, the plasma is diverted around the obstacle and a dense, turbulent layer — the magnetosheath — forms in front of it. We study instances of fast plasma jets bursting through the shock and traveling towards Earth. However, it appears that only a small proportion of jets hit the edge of our magnetic field — the magnetopause. To forecast their effects, we therefore need to know when jets will make it through. We use a database of 13,096 jets observed by spacecraft in the magnetosheath, alongside measurements of the solar wind, to determine when jets are most likely to hit the magnetopause. We find the highest probability is when the solar wind magnetic field is aligned with its flow direction and when it has a higher speed. We hope that, with this information, we may eventually be able to forecast space weather effects of jets based solely on measurements of the upstream solar wind.

1 Introduction

Magnetosheath jets, also referred to as 'high-speed jets' (HSJs; Plaschke et al., 2013), 'dynamic pressure enhancements' (Archer & Horbury, 2013), or 'plasmoids' (Karlsson et al., 2015) (hereafter referred to simply as 'jets'), are localized high-dynamic pressure pulses observed in the magnetosheath (see Plaschke et al., 2018, and references therein for a comprehensive review). Jets are seen approximately 9 times more often downstream of the quasi-parallel shock, that is, where the angle between the interplanetary magnetic field (IMF) and the local shock normal is less than 45°, than the quasi-perpendicular shock (Archer & Horbury, 2013; Plaschke et al., 2013; Vuorinen et al., 2019). Recently, Raptis et al. (2020) studied the differences between jets found downstream of the quasi-parallel shock versus those arising at the quasi-perpendicular shock, finding that they display different properties, with quasi-perpendicular jets being generally weaker in terms of velocity, density, and duration. This is in line with suggestions of differing formation processes. One theory is that jets originate from the non-uniform processing of solar wind plasma through ripples in the bow shock surface and propagate earthward (Hietala et al., 2009, 2012). Ripples are generally thought to be the result of foreshock structures impacting the shock (e.g, Schwartz & Burgess, 1991), hence this is a prominent mech-

anism at the quasi-parallel shock. In addition, there is evidence to suggest that some jets may form from the interaction of foreshock short large-amplitude magnetic structures (SLAMS) with bow shock ripples (Karlsson et al., 2015; Palmroth et al., 2018; Raptis et al., 2020). Several other formation mechanisms have been proposed, some of which may explain jets observed downstream of the quasi-perpendicular shock, such as rotational discontinuities in the IMF (Archer et al., 2012; Dmitriev & Suvorova, 2012).

As they propagate into the magnetosheath, generally at higher velocities than their surroundings, magnetosheath jets can disturb the local plasma environment by driving bow waves and secondary particle accelerating shocks ahead of them (e.g., Liu et al., 2020). If jets go on to hit the magnetopause they may produce magnetospheric effects. As their dynamic pressure is enhanced with respect to the surrounding magnetosheath, they can indent and rebound from the magnetopause surface (Amata et al., 2011; Dmitriev & Suvorova, 2015; Shue et al., 2009), launch propagating waves (Plaschke et al., 2009; Archer et al., 2014), or create surface eigenmodes, as was theorized by Plaschke et al. (2009) and recently observed by Archer et al. (2019). In addition, the increased dynamic pressure they present can compress the magnetopause current sheet, stimulating magnetic reconnection. This was observed by Hietala et al. (2018) who reported in situ observations of reconnection triggered by a jet impact. They saw that, despite favorable conditions in terms of magnetic field alignment and β-shear (see, e.g., Swisdak et al., 2010), reconnection was prevented by the magnetopause layer being too thick. However, following a jet impact, this layer was sufficiently compressed that reconnection onset was observed. In another case study, Nykyri et al. (2019) inferred that a substorm was triggered by a jet bringing southward B_Z to the magnetopause during a period of northward IMF. A number of other potential interactions have been studied. For example, Dmitriev and Suvorova (2015) suggested that jets may stimulate impulsive penetration of magnetosheath plasma into the magnetosphere, while Wang et al. (2018) observed that jet impacts may be linked to auroral brightenings.

The aforementioned effects involve the interaction of jets with the magnetopause. Jets are believed to impinge upon the magnetopause very often: Large scale magnetosheath jets, with a cross-sectional diameter of $2\,\mathrm{R_E}$ or greater, have been estimated to impact the magnetopause several times per hour, with smaller jets potentially impacting hundreds or thousands of times per hour (Plaschke et al., 2016; Plaschke, Hietala, & Vörös, 2020). Therefore, in order to eventually forecast magnetospheric effects arising from jets, we must first establish when jets are most likely to impact the magnetopause. In their statistical study, Plaschke et al. (2013) determined that jets are most commonly observed near and shortly downstream of the bow shock, with the probability of observation falling dramatically close to the magnetopause, suggesting that they are often dissipated, braked, or broken up during propagation. This idea has been supported by simulations such as those by Karimabadi et al. (2014) and Omidi et al. (2016) where jets have been seen to face instabilities and turbulence during their propagation. In addition, a recent study by Palmroth et al. (2021) combined jet observations from the Magnetospheric Multiscale spacecraft (MMS; Burch et al., 2016) with global hybrid-Vlasov simulations to examine how jet properties evolve as they propagate. They found that the jet's density, dynamic pressure, and magnetic field magnitude all fall from the bow shock to the magnetopause, while temperature rises, making near-magnetopause jets more akin to the surrounding plasma.

Despite their potential magnetospheric effects, there has been relatively little work to date on understanding what controls jet propagation, particularly with respect to the upstream solar wind and forecasting. One suggestion was made by Goncharov et al. (2020), by simple comparison of observed jet distances from a model bow shock, that jets propagate deeper into the magnetosheath downstream of the quasi-parallel shock than downstream of the quasi-perpendicular shock. In the subsolar region of the magnetosheath this corresponds to low cone angle solar wind, which is now also a well-established fa-

vorable condition for jet formation, with minor dependencies on solar wind speed, density, and IMF stability noted by Plaschke et al. (2013) and Archer and Horbury (2013).

The focus of the present work is, therefore, on determining what upstream solar wind conditions are most favorable for large numbers of jets to reach and impact the magnetopause, with a view to informing future forecasting regimes. We further break this problem down into two components: probability of jet formation at the bow shock, and probability of unimpeded propagation to the magnetopause. We consider these two processes separately, as it is not immediately obvious whether, for a given solar wind quantity, they would reinforce or counteract each other. When combined, the net effect paints a picture of how different solar wind conditions affect the overall rate of jets reaching the magnetopause. Using a large data set of jets observed over 11 years, with a variety of corresponding upstream solar wind conditions, we statistically determine the most favorable conditions to be those associated with the fast solar wind, with low IMF cone angle and high solar wind speed being the most strongly controlling properties. We see weak dependencies on IMF magnitude, Alfvén Mach number, and density, while plasma beta and solar wind dynamic pressure have no net effect.

In the next section we introduce the data set used in this study and describe our analysis techniques. In Section 3 we present the results of our analyses on jet formation and propagation, with their combined significance discussed in Section 4. Finally, in Section 5 we summarize our findings and make suggestions for future work.

2 Data and Methods

2.1 Data Set

In this study we make use of a database of 13,096 jet observations made by the five Time History of Events and Macroscale Interactions during Substorms spacecraft (THEMIS; Angelopoulos, 2008) from 2008 to 2018 (inclusive) (data are available from Plaschke, Hietala, & Angelopoulos, 2020; Plaschke, Hietala, & LaMoury, 2020). Jets are selected from over 31 million (8713.5 hours) magnetosheath measurements. The full data set is presented here for the first time, though it should also be noted that it contains the 2,859 jets first presented by Plaschke et al. (2013), and was compiled using the same methods as that study. We give some comparative statistics for each data set in Table 1. For a full description of the algorithmic detection we therefore refer the reader to Plaschke et al. (2013), but here we shall summarize the key points relevant to this work. Intervals where a THEMIS probe was determined to be in the subsolar (within a 30° cone with Earth at the tip, symmetrical about the Sun-Earth line) magnetosheath for at least two continuous minutes are initially selected via density and radial distance criteria. THEMIS data are interpolated such that all measurements share a common one second cadence. Each measurement in the magnetosheath is then associated with upstream solar wind conditions taken from the OMNI database (King & Papitashvili, 2005), averaged for the preceding five minutes. From these intervals, jets are identified as instances where the maximum X_{GSE}-directed dynamic pressure measured in the magnetosheath exceeds half that of the pristine solar wind. We use this criterion as it is most relevant for forecasting magnetopause impacts. Leading and trailing edges of each jet are defined as the closest points either side of the maximum where dynamic pressure drops below a quarter of the solar wind value. Note, however, that the analysis presented in this study considers only the solar wind conditions associated with the point of maximum dynamic pressure within each jet.

We extend the database of Plaschke et al. (2013) for several reasons. The aim of this study is to make a step towards understanding and forecasting the space weather effects of jets. Naturally, space weather studies are generally concerned with extreme events, with many effects showing some kind of solar cycle dependence. It is therefore crucial

Table 1. Comparison of key statistics between data sets.

Property	2008–2011	2012–2018	2008–2018
Number of jets	2,859	10,237	13,096
Magnetosheath data (hours)	2,736.9	6,212.5	8,949.4
Magnetosheath data outside model boundaries	13 %	12 %	12 %
Jets outside model boundaries	202 (7 %)	375 (4 %)	577 (4 %)
Jets $F < 0.25$ (near MP)	678	1,256	1,924
Jets $F > 0.75$ (near BS)	313	1,426	1,739

Note. Data from 2008–2011 were first introduced by Plaschke et al. (2013), while those from 2012–2018 are presented here for the first time. This study makes use of both data sets combined (last column). F is the fractional distance through the model magnetosheath, as described in the text.

to obtain a data set spanning a whole solar cycle, extending the four years around solar minimum covered by Plaschke et al. (2013). For example, from 2008 to 2011, only 12 % (328 hours) of magnetosheath data corresponded to upstream solar wind speeds of above 500 km s^{-1} with a maximum observed speed of 736 km s^{-1}, compared to 23 % (1433 hours) and a maximum of 846 km s^{-1} in the 2012–2018 data set, which contains the solar maximum.

The variable dynamic pressure of the solar wind causes the magnetopause and bow shock positions to fluctuate, altering the thickness of the magnetosheath layer. Therefore, in order to meaningfully compare factors affecting jet propagation through the magnetosheath, we place each observation on a normalized relative distance scale. This is calculated by

$$F = \frac{R - R_{\mathrm{MP}}}{R_{\mathrm{BS}} - R_{\mathrm{MP}}}, \tag{1}$$

where R is the radial distance of the spacecraft from Earth, R_{MP} the radial distance to a model magnetopause, and R_{BS} the radial distance to a model bow shock, such that $F = 1$ at the bow shock and 0 at the magnetopause (Archer & Horbury, 2013). The models used for the magnetopause and bow shock are those by Shue et al. (1998) and Merka et al. (2005) respectively, and solar wind conditions from OMNI are used as model inputs.

Figure 1 shows the distribution of jet observation positions within this one-dimensional model magnetosheath. Figure 1a shows the 2,859 jets presented by Plaschke et al. (2013), Figure 1b shows the new data set containing 10,237 jets measured by THEMIS from 2012 to 2018 (inclusive), while Figure 1c shows these two data sets combined. In each, the blue histogram shows the locations of jet measurements within the model magnetosheath, which is generally seen to peak in the middle, around $F = 0.5$. The red histograms give the equivalent location of all the magnetosheath intervals from which the jets were selected, peaking nearer $F = 0$, indicating that the THEMIS probes were generally close to the magnetopause in this time period. This would, naturally, increase the number of jets observed near the magnetopause, and decrease the number observed near the bow shock, skewing potential conclusions. To account for this bias, we divide the jet distributions (blue) by the magnetosheath distributions (red) and re-normalize, thus removing the orbital effects. The resulting distributions are shown in black and are expressed in units of jets observed per hour spent in the magnetosheath, per bin. Error bars are estimated using the Clopper-Pearson method to calculate a 95 % binomial confidence interval, and therefore are larger when there are fewer data in a given bin (e.g., Brown et al., 2001). It is important to note that this normalization technique is used throughout the rest of this study, such that we deal with 'true' distributions, free of biases arising from non-

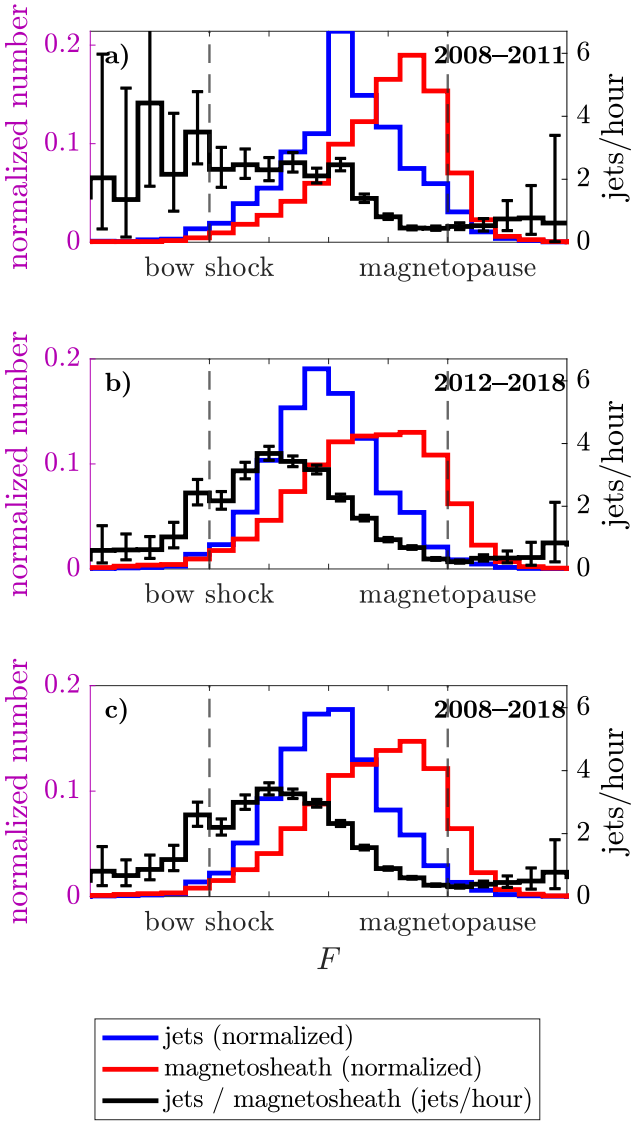

Figure 1. Distributions of observation locations through model magnetosheath. Jet observations are shown in blue and the magnetosheath reference distribution in red. Both are normalized for ease of comparison. The black histograms give the unbiased probability distributions accounting for orbital effects, expressed in units of jets observed per hour spent in the magnetosheath. a) THEMIS measurements from 2008–2011, as presented by Plaschke et al. (2013); b) new data set from 2012–2018; c) both data sets combined.

uniform sampling of the parameter space. Figure 1 therefore implies that jets are most likely to be observed downstream of the bow shock, with the probability of observation dropping towards the magnetopause. This is consistent with the idea that they are formed from the interaction of solar wind with bow shock ripples (Hietala et al., 2009, 2012). As we are concerned with understanding what allows jets to propagate from the bow shock to the magnetopause, we require a sufficient number of jet observations near these boundaries. Herein, we therefore make use of the combined data set as whole, making no distinction between the older and newer data.

There is some amount of uncertainty regarding a jet's exact location with respect to the boundaries. As shown in Table 1, 4 % of jet observations and 12 % of magnetosheath intervals fall outside of our model boundaries despite the fact that the selection criteria are such that all data are believed to be truly from the magnetosheath. Though commonly used, the empirical models may have limitations. For example, Suvorova et al. (2010) suggested that, under prolonged periods of quasi-radial IMF, the true magnetopause position may lie significantly further out than what is predicted by the Shue et al. (1998) model. To account for these uncertainties, we will keep our bin size coarse (one quarter of the model magnetosheath thickness). The models are driven by data from OMNI, which naturally contain some uncertainty as they are algorithmically propagated to the bow shock from measurements at L1, meaning they do not necessarily represent the true solar wind conditions at the shock surface at the time of formation. We do not consider this to be a significant issue, however, as any forecasting regime developed from our results would likely encounter the same limitations.

2.2 Investigating Solar Wind Control of Jet Formation and Propagation

To understand what affects the probability of jet formation, we use the database to produce probability distributions showing the likelihood of observing a jet near the bow shock as a function of relevant solar wind parameters. As with Figure 1, we normalize jet distributions by the corresponding distribution for magnetosheath measurements, thus highlighting how typical upstream solar wind conditions for jet formation differ from the norm. Note that a similar analysis was performed by Plaschke et al. (2013). A crucial difference here, however, is that we restrict our analysis to only jets and magnetosheath observations made near the bow shock (those with $F > 0.75$) so that potential differences in jet propagation probability do not influence conclusions on factors affecting jet formation.

To be geoeffective, jets must interact with the magnetopause. It is therefore important to determine why some jets are able to travel further than others, and, with a particular view to forecasting, what solar wind conditions lead to the formation of jets that are more likely to propagate through the magnetosheath and reach the magnetopause. We approach this problem via two analysis techniques, which are illustrated in Figure 2 where we show a cartoon of the parameter space to be explored.

If jet propagation depth is dependent on a particular solar wind parameter, we would expect to see a change in the distribution of this parameter during jet observations at different depths into the magnetosheath (different values of F). Our first method for establishing how the solar wind conditions affect jet propagation is, therefore, to compare the solar wind parameter probability distributions for newly formed jets close to bow shock ($F > 0.75$, the region highlighted in green in Figure 2), with jets observed reaching the magnetopause ($F < 0.25$, green). Differences between the two distributions may indicate that the solar wind quantity in question has an influence on the ability of a jet to propagate to the magnetopause.

The second approach taken was to compare relative distance (F) distributions (as in Figure 1) filtered by extreme values of each solar wind parameter. These can be in-

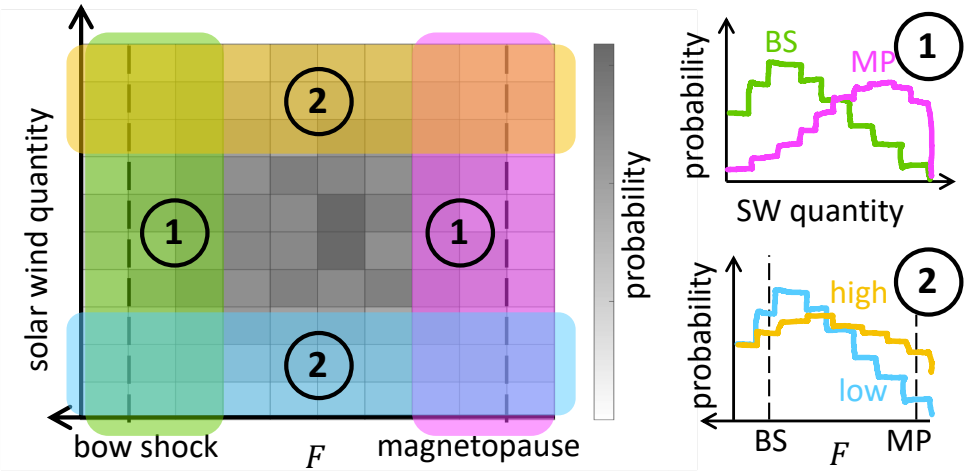

Figure 2. Cartoon of the parameter space explored to determine how solar wind conditions affect jet propagation. In method 1, normalized probability distributions of solar wind quantities are compared for near-bow shock (green region) and near-magnetopause (magenta) jets. In method 2, normalized probability distributions in F are compared for high (orange) and low (cyan) values of each solar wind quantity.

terpreted as the orange and cyan regions in Figure 2. Threshold values were chosen as those that best captured a difference in the two populations, without limiting to too few observations (i.e., without increasing the size of the error bars). As jet occurrence falls from the bow shock to the magnetopause, we expect most distributions to broadly follow this trend. A difference in gradient between the two distributions, however, implies that a solar wind quantity may influence expected jet propagation depth. If a particular solar wind condition is highly favorable for jet survival, the flatter we expect its distribution to be.

3 Results

3.1 Factors Affecting Jet Formation

Figure 3 shows probability distributions for jet formation at the bow shock as a function of each solar wind parameter studied. As mentioned previously, these are comparable with the analyses of Plaschke et al. (2013), except that we restrict to only jets and magnetosheath data recorded near the bow shock ($F > 0.75$) so as to isolate factors affecting jet formation from other effects that may influence the likelihood of jet observation. As in Figure 1, blue histograms represent raw jet observations and red histograms are the reference distributions for magnetosheath data. Green histograms (those with error bars) show the unbiased probability distributions.

From the green curve in Figure 3a, we see that jet formation is highest during low IMF cone angle solar wind. This is in agreement with the findings of Plaschke et al. (2013) who, with their smaller data set, concluded that cone angle was the only strongly controlling factor, but noted weak dependencies on density and wind speed. We see solar wind speed (Figure 3b) to display an interesting bipolar signature, with an upward trend towards low speeds but an additional and significant peak around 600 $\mathrm{km\,s^{-1}}$. This pattern is not dissimilar to what was seen by Archer and Horbury (2013), particularly down-

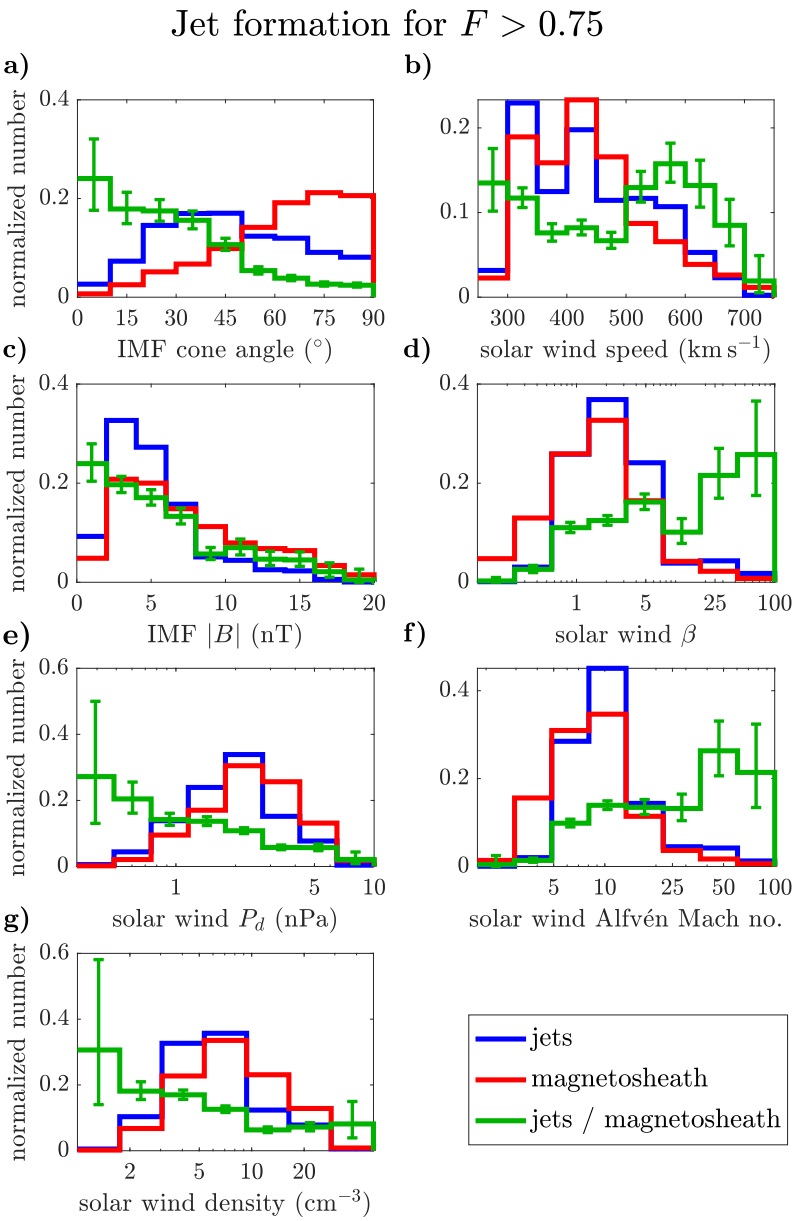

Figure 3. Distributions of upstream solar wind conditions, illustrating how they affect the probability of jets forming at the bow shock. Observations associated with jets are shown in blue, magnetosheath reference distribution in red, and the normalized distributions (those with error bars) in green. All observations are restricted to $F > 0.75$, i.e., near the bow shock, corresponding to the green region of Figure 2. Solar wind quantities shown are: a) IMF cone angle; b) solar wind speed; c) IMF magnitude; d) solar wind plasma beta (log scale); e) solar wind dynamic pressure (log scale); f) solar wind Alfvén Mach number (log scale); g) solar wind density (log scale).

stream of the quasi-parallel shock. Low IMF $|B|$ (Figure 3c), high β (Figure 3d), low dynamic pressure (Figure 3e), and high Alfvén Mach number (Figure 3f), also appear to promote jet formation. From Figure 3g it does indeed appear that jets are more likely to form during low density wind, arguably displaying a more than minor dependence. The results for Alfvén Mach number and β are in agreement with the recent conclusions of Goncharov et al. (2020), though they found the opposite result for the IMF magnitude. It should be noted, however, that their data set was significantly smaller (1,400 jets) than this present study, and they did not distinguish between formation and propagation effects.

3.2 Factors Affecting Jet Propagation

Figure 4 shows the first technique used to determine the effect of solar wind conditions on jet propagation. The overlaid histograms show the distributions of solar wind parameters for jets observed close to the magnetopause ($F < 0.25$, magenta) of which there are 1,924, compared with jets observed near the bow shock ($F > 0.75$, green) of which there are 1,739. IMF cone angle (Figure 4a) appears to be a controlling factor for jet propagation, with jets observed near the magnetopause showing an even stronger preference to occur during low cone angles than near-bow shock jets. Solar wind speed (Figure 4b) shows a very clear split, with jets observed near the bow shock recording far slower upstream solar wind speeds than jets near the magnetopause, implying that jets formed during faster wind will be more likely to reach the magnetopause. The distributions in Figures 4c, 4d, 4f, and 4g, representing IMF magnitude, plasma beta, Alfvén Mach number, and density, respectively, lie roughly on top of each other, overlapping in their error bars and showing no clear skew. This suggests that, within uncertainty, they have no effect on jet propagation. Figure 4e, showing solar wind dynamic pressure, indicates that jets observed near the bow shock are generally formed of low dynamic pressure solar wind while jets at the magnetopause are formed from a range of dynamic pressures. This creates a separation in the upper region of the scale, suggesting that high dynamic pressure solar wind creates jets more likely to reach the magnetopause. This makes sense given the clear dependence on solar wind speed.

Figure 5 shows jet F distributions separated by high and low values of each solar wind parameter, our second technique used to investigate jet propagation. The potential factors identified in the previous subsection — low IMF cone angle (Figure 5a), high solar wind speed (Figure 5b), and dynamic pressure (Figure 5e) — all show clear confirmation of their influence, with the two distributions showing clear separation. Figure 5a provides a broader statistical backing for the assertion made by Goncharov et al. (2020) that jets propagate further into the magnetosheath downstream of the quasi-parallel shock. In addition, Figures 5c and 5d suggest that, according to this analysis technique, higher IMF $|B|$ and low solar wind beta may in fact promote jet propagation. These factors did not produce a noticeable effect via the first technique. The solar wind density (Figure 5g) does not show a clear effect.

4 Discussion

Thus far we have considered the solar wind control of jet formation and jet propagation separately. For example, we have seen that a low IMF magnitude is favorable for the creation of jets (Figure 3c), but also that a higher IMF magnitude increases the likelihood of a jet surviving from the bow shock to the magnetopause (Figure 5c). On first glance, these two statements may seem contradictory but it is in fact possible for a solar wind parameter to affect jet formation and propagation differently. However, our results so far give us no information as to the relative magnitudes of these effects, or which regime might dominate. To address this, we present Figure 6 which, like Figure 5, shows F distributions separated by high and low threshold values of each solar wind param-

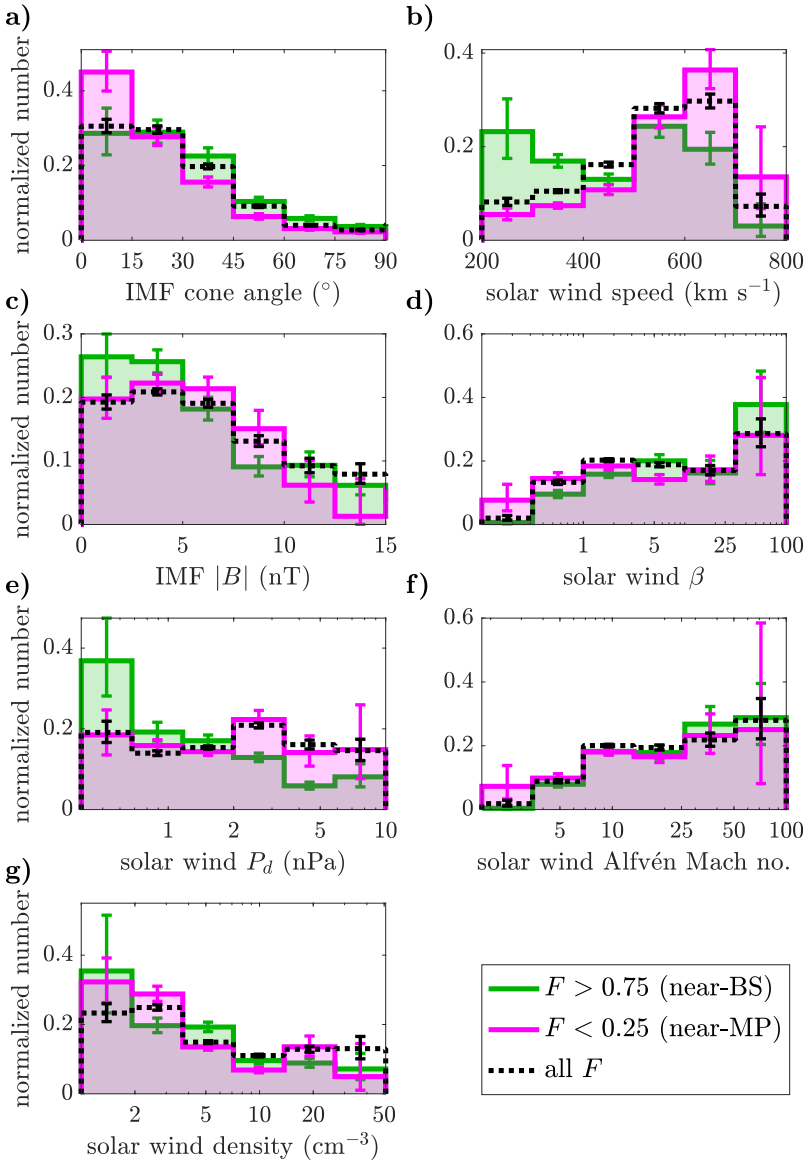

Figure 4. Distributions of upstream solar wind properties for jets, separated by near-bow shock ($F > 0.75$, green) and near-magnetopause ($F < 0.25$, magenta) jets. Distribution for all F values shown with a black dotted line. a) IMF cone angle; b) solar wind speed; c) IMF magnitude; d) solar wind plasma beta (log scale); e) solar wind dynamic pressure (log scale); f) solar wind Alfvén Mach number (log scale); g) solar wind density (log scale).

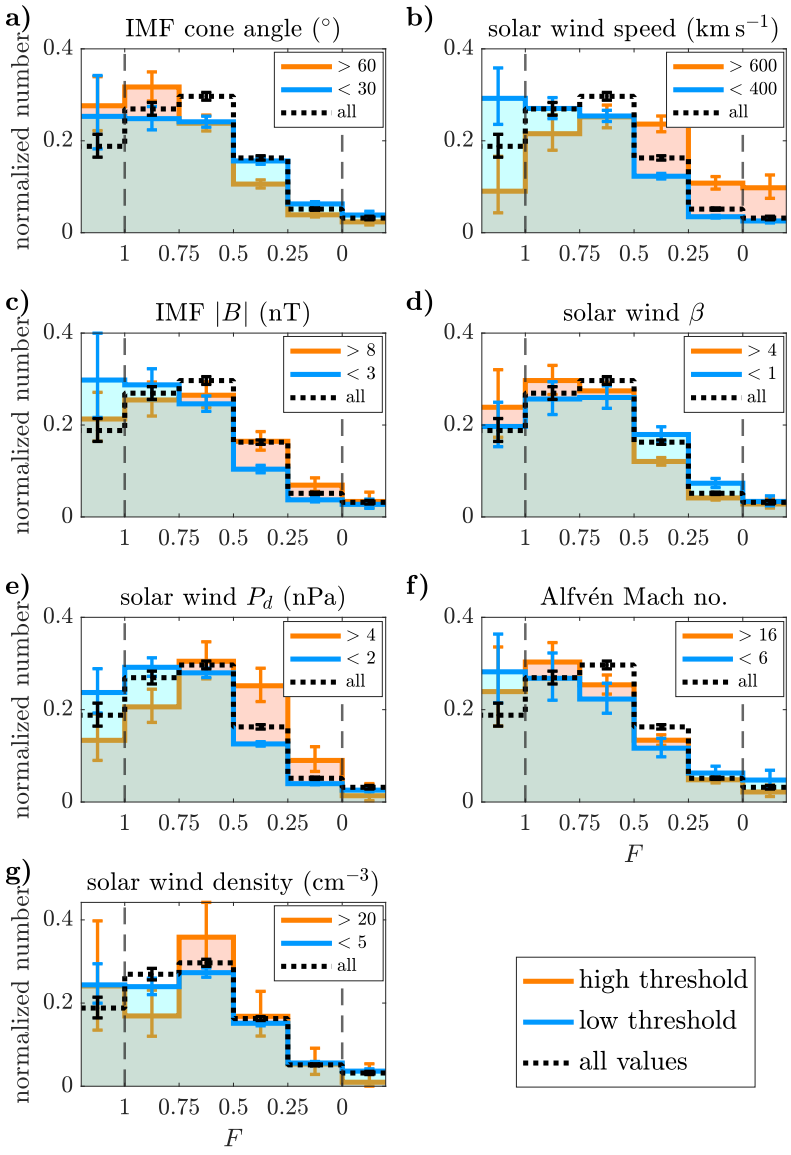

Figure 5. Normalized distributions of jet observation locations in model magnetosheath, separated by high and low threshold values of upstream solar wind parameters. In each, orange histograms are for jets observed with solar wind conditions above a high threshold, while cyan distributions represent those below a low threshold. Unconstrained distributions shown with a black dotted line. a) IMF cone angle; b) solar wind speed; c) IMF magnitude; d) solar wind plasma beta; e) solar wind dynamic pressure; f) solar wind Alfvén Mach number; g) solar wind density.

eter. The key difference here, however, is that, instead of simply normalizing, we express histograms in units of jets observed per hour the spacecraft spent in the magnetosheath, within each F bin, under those solar wind conditions. This combines both formation and propagation effects, enabling us to extract the rates of jets reaching the magnetopause under different solar wind conditions. The dashed black curves show the F distributions unconstrained by solar wind conditions and are therefore representative of the black curve in Figure 1c (though with different binwidth). This allows us to see how each jet subset observed under constrained solar wind conditions compares to the general population, and the factors that most strongly contribute to the shape of the curve. Note also that by comparing the left side of each plot (in particular for $0.75 < F < 1$) we can clearly see the factors influencing jet formation rates at the bow shock (as explored in Figure 3).

The cyan histogram in Figure 6a, representing low cone angles, dwarfs its high cone angle counterpart throughout all regions of the magnetosheath showing that, as expected from the preceding results, jets are far more likely to reach the magnetopause under low cone angle solar wind than high cone angle solar wind. A similar, but not as strong, combined effect is seen for solar wind speed in Figure 6b. Quantities that display oppositely directed formation and propagation effects are particularly interesting. In Figure 6c we can see that for low IMF magnitude solar wind there are significantly more jets formed at the bow shock. However, due to the propagation effects described in Section 3.2, the observation rate falls far faster than the high IMF magnitude solar wind such that near the magnetopause the occurrence rate of jets formed from low IMF magnitude solar wind is only marginally higher than for high IMF magnitudes. This cancellation effect is even clearer in solar wind plasma beta (Figure 6d) and dynamic pressure (Figure 6g), and so both can be said to have no overall effect on the rate of jets reaching the magnetopause.

In Table 2 we quantify these effects and give numerical comparisons of jet observation rates at the magnetopause for high and low values of each solar wind parameter. These statistics are drawn from the difference in height of the $0 < F < 0.25$ bars in each panel of Figure 6. Note that we do not place emphasis on the absolute values in jets per hour (though these can be read from Figure 6), as our selection criteria are such that smaller jets are more likely to be missed (Plaschke, Hietala, & Vörös, 2020), and our observation window is confined to the subsolar region. However, the relative observation rates under different solar wind conditions give clear indicators as to what factors are most relevant for magnetopause impacts. We therefore provide quantitative estimates for how the changing solar wind conditions affect the likelihood of jets reaching the magnetopause. IMF cone angle is the strongest controlling factor overall, with nearly 12 times as many jets expected to reach the magnetopause under low ($< 30°$) angles than under high ($> 60°$) angles. This factor is more extreme than the factor of 9 disparity in jet occurrence rate observed by Vuorinen et al. (2019) due to the compounding of formation and propagation effects. The next largest is solar wind speed, where we see 4.7 times as many jets in front of the magnetopause when the solar wind is fast ($> 600\,\mathrm{km\,s^{-1}}$) compared to when it is slow ($< 400\,\mathrm{km\,s^{-1}}$). The influences of low IMF magnitude, high Alfvén Mach number, and low density are more minor in comparison but still notable, each making jet impacts approximately twice as likely as their opposite conditions. This analysis is somewhat sensitive to the exact values chosen to define 'high' and 'low' thresholds, meaning that the values shown in the last column of Table 2 should only be taken as approximate indicators of the scale of each effect. The general conclusions, however, remain intact regardless of the choice of threshold values. The only parameters examined in this study that show no clear net effect on the likelihood of jets reaching the magnetopause are the solar wind dynamic pressure and plasma beta.

Our analysis is subject to some limitations and caveats. If jets are braked during propagation, they may be slowed to the point that they are no longer detectable via our jet selection criteria (that their earthward dynamic pressure exceeds half that of the pris-

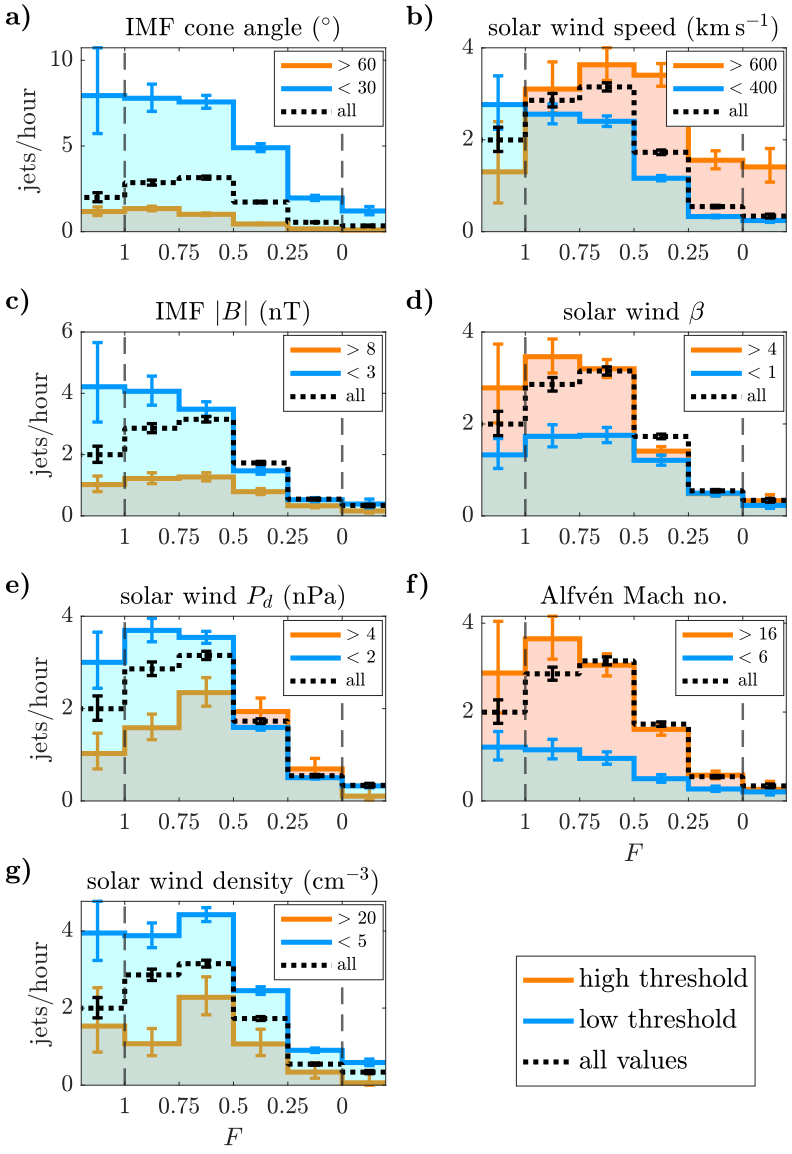

Figure 6. Same format as Figure 5 except that distributions are not normalized and are instead expressed in units of jets per hour per bin spent in the magnetosheath for each restricted distribution, thus combining formation and propagation effects The net effect on the number of jets reaching the magnetopause is calculated from the $0 < F < 0.25$ column. a) IMF cone angle; b) solar wind speed; c) IMF magnitude; d) solar wind plasma beta; e) solar wind dynamic pressure; f) solar wind Alfvén Mach number; g) solar wind density.

Table 2. Summary of effects of solar wind conditions on the numbers of jets expected to reach the magnetopause.

Solar wind parameter	High	Low	Influence on jets reaching magnetopause
Cone angle (°)	> 60	< 30	11.8 times more during low cone angle
Speed ($\mathrm{km\,s^{-1}}$)	> 600	< 400	4.7 times more during high speed
IMF $\lvert B\rvert$ (nT)	> 6	< 3	1.6 times more during low $\lvert B\rvert$
Beta	> 4	< 1	No net effect
Dynamic Pressure (nPa)	> 4	< 2	No net effect
Alfvén Mach number	> 16	< 6	2.2 times more during high Mach number
Density ($\mathrm{cm^{-3}}$)	> 20	< 5	2.7 times more during low density

Note. All statistics derived from jet observations with $0 < F < 0.25$, i.e., immediately in front of the magnetopause. Threshold values are those used to define 'high' and 'low' populations in Figures 5 and 6.

tine solar wind). This, in part, may explain the drop-off that is seen in the black curves of Figure 1, potentially exaggerating the gradient if a number of weakened jets continue to propagate undetected. Similarly, Plaschke, Hietala, and Vörös (2020) suggested that jets can fragment into several smaller jets (or merge into larger ones) as they travel, changing their cross-sectional areas, and thus the likelihood of being observed by a single spacecraft. This raises questions about where is an appropriate level to set the detection threshold, i.e., how small or slow does a jet have to become before it is no longer considered a jet? While an interesting problem, we do not consider it an issue as the focus of this study is understanding the conditions most relevant for magnetopause impacts. We are, therefore, most interested in larger and faster jets observed near the magnetopause, i.e., those with a greater chance of being geoeffective, which our selection criteria are most likely to capture. Note also that we do not observe jets actually impacting the magnetopause. However, we find it reasonable to assume that a jet observed immediately in front of the magnetopause will later go on to strike it. We propose that a dedicated study of magnetopause crossings should be performed to build a database of jet impacts and catalog their effects on the surrounding plasma environment.

A potential explanation for higher solar wind dynamic pressures increasing the likelihood of jets propagating far into the magnetosheath can be reached by considering jet travel times. Under high dynamic pressure conditions, the magnetosheath layer is compressed and thinned, decreasing the time taken for a jet to reach the magnetopause. Similarly, we see that higher solar wind speed creates faster jets (though this is, to an extent, necessitated by our selection criteria), which are then able to reach the magnetopause in less time. This could lower the chance of a jet being broken up, though it is unlikely to be the only factor affecting the dissipation rate. Further study should, therefore, be conducted into how jets interact with instabilities and dissipation mechanisms.

Many of the solar wind properties studied are related. Fast solar wind is generally expected to have a lower density and a more radial magnetic field (i.e., lower cone angle), though it is generally seen to have a lower Alfvén Mach number than slow solar wind (see, e.g, Ebert et al., 2009). As fast solar wind is seen at the equator more often in times near solar maximum (e.g., McComas et al., 2003) there may therefore be a solar cycle dependence for jets impacting the magnetopause. This may explain the differences between the two data sets in terms of jet occurrence rates and distributions in F (i.e., between Figure 1a and 1b), as the former was compiled around a deep solar minimum, while the latter included solar maximum.

Our results also suggest that it may be interesting to study magnetosheath jets as a response to extreme solar wind transients. Coronal mass ejections (CMEs) are typically observed with higher speeds, densities, and magnetic field magnitudes than the ambient solar wind at 1 AU (e.g., Kilpua et al., 2017). Based on our findings, CMEs may enhance the rates of jets reaching the magnetopause by virtue of their speed, though increased density may work to counteract this. Increased magnetic field strength may reduce the absolute numbers of jets formed at the bow shock, but the likelihood of their survival to the magnetopause will be increased such that the rates of jets reaching the magnetopause are largely unaffected by the magnetic field magnitude itself. The potential effects may even extend beyond those arising directly from the magnetic cloud itself. Neugebauer et al. (1997) observed that extended periods of radial IMF often follow in the wake of a CME. This idea sets up an interesting scenario where jet production and propagation could be increased both during a CME impact and in the hours following it.

Analysis by Turc et al. (2018, 2019) showed through global simulations and Cluster observations that a higher IMF $|B|$ causes foreshock waves to move to smaller spatial scales, which in turn creates smaller ripples on the quasi-parallel bow shock, increasing the number of potential sites for jet formation. Our results appear in contradiction to this, where we see that higher magnetic field magnitudes actually decrease the likelihood of jet formation (Figure 3c). However it may be the case that smaller ripples create more, but smaller, jets that are less likely to be detected by a single spacecraft. More targeted research into the effects of CMEs on magnetosheath jets is needed. Naturally, this also applies to other solar wind transients such as stream interaction regions (SIRs) and corotating interaction regions (CIRs) that present increased speeds and so would also be expected to have an effect on the rate of jet production and propagation (Jian et al., 2006).

5 Summary and Conclusion

Using a new database of 13,096 jets seen by the THEMIS spacecraft from 2008 to 2018 we have performed statistical analysis to determine how upstream solar wind conditions (obtained from OMNI) affect the likelihood of jets forming at the bow shock and then propagating to the magnetopause without dissipating. We find that a number of parameters increase the likelihood of jets forming at the bow shock, the most favorable conditions being: low IMF cone angle, solar wind speeds of $\sim 300\,\mathrm{km\,s^{-1}}$ or $\sim 600\,\mathrm{km\,s^{-1}}$, low IMF magnitude, high beta, low dynamic pressure, high Alfvén Mach number, and low density. We find that once jets are formed at the bow shock, their likelihood of surviving throughout propagation to the magnetopause is also controlled by the upstream solar wind conditions. The conditions most favorable for this are: low IMF cone angle, high solar wind speed, high IMF magnitude, low beta, and high dynamic pressure. Combining these two effects, we find that higher numbers of jets reach, and therefore likely impact, the magnetopause when the solar wind exhibits a low IMF cone angle, high wind speed, high Alfvén Mach number, and low density. Solar wind beta and dynamic pressure display no net effect on the rates of jets reaching the magnetopause.

It is notable that several of these properties are associated with fast solar wind and extreme solar wind transient events, and therefore may be modulated by the solar cycle. Under these solar wind conditions the highest impact rates of jets on the magnetopause are expected, increasing the likelihood of them affecting magnetospheric dynamics and potentially inducing space weather effects. Many opportunities for future work are apparent. We suggest a targeted study on the relation of jets and solar wind transients be performed, as well as further investigation into the properties of near-magnetopause jets and their interactions with the magnetopause. We hope that these findings will provide a useful step towards eventual space weather forecasting regimes whereby we will be able

to predict the inner-magnetosphere effects of magnetosheath jets purely from measurements of the solar wind upstream of the bow shock.

Acknowledgments

ATL and HH were supported by Royal Society awards URF\R1\180671 and RGF\EA\181090. FP was supported by the Austrian Science Fund (FWF): P 33285-N. LV acknowledges the financial support of the Academy of Finland (Project #309939) and of the University of Turku Graduate School. JPE was supported by UKRI/STFC grant ST/S000364/1. THEMIS and OMNI data can be accessed using the SPEDAS software (Angelopoulos et al., 2019). Jet and magnetosheath interval times are available at `https://osf.io/gf732/` (2008–2011; Plaschke, Hietala, & Angelopoulos, 2020) and `https://osf.io/7rjs4/` (2012–2018; Plaschke, Hietala, & LaMoury, 2020).

References

Amata, E., Savin, S., Ambrosino, D., Bogdanova, Y., Marcucci, M., Romanov, S., & Skalsky, A. (2011). High kinetic energy density jets in the earth's magnetosheath: A case study. *Planetary and Space Science*, *59*(7), 482 - 494. doi: 10.1016/j.pss.2010.07.021

Angelopoulos, V. (2008). The THEMIS mission. *Space Science Reviews*, *141*(1-4), 5–34. doi: 10.1007/s11214-008-9336-1

Angelopoulos, V., Cruce, P., Drozdov, A., Grimes, E. W., Hatzigeorgiu, N., King, D. A., ... Schroeder, P. (2019). The Space Physics Environment Data Analysis System (SPEDAS). *Space Science Reviews*, *215*(1), 9. doi: 10.1007/s11214-018-0576-4

Archer, M. O., Hietala, H., Hartinger, M. D., Plaschke, F., & Angelopoulos, V. (2019). Direct observations of a surface eigenmode of the dayside magnetopause. *Nature Communications*, *10*(1), 615. doi: 10.1038/s41467-018-08134-5

Archer, M. O., & Horbury, T. S. (2013). Magnetosheath dynamic pressure enhancements: Occurrence and typical properties. *Annales Geophysicae*, *31*(2), 319–331. doi: 10.5194/angeo-31-319-2013

Archer, M. O., Horbury, T. S., & Eastwood, J. P. (2012). Magnetosheath pressure pulses: Generation downstream of the bow shock from solar wind discontinuities. *Journal of Geophysical Research: Space Physics*, *117*(5), 1–13. doi: 10.1029/2011JA017468

Archer, M. O., Turner, D. L., Eastwood, J. P., Horbury, T. S., & Schwartz, S. J. (2014). The role of pressure gradients in driving sunward magnetosheath flows and magnetopause motion. *Journal of Geophysical Research: Space Physics*, *119*(10), 8117–8125. doi: 10.1002/2014JA020342

Brown, L. D., Cai, T. T., & DasGupta, A. (2001). Interval estimation for a binomial proportion. *Statistical Science*, *16*(2), 101 – 133. doi: 10.1214/ss/1009213286

Burch, J. L., Moore, T. E., Torbert, R. B., & Giles, B. L. (2016). Magnetospheric Multiscale overview and science objectives. *Space Science Reviews*, *199*(1-4), 5–21. doi: 10.1007/s11214-015-0164-9

Dmitriev, A. V., & Suvorova, A. V. (2012). Traveling magnetopause distortion related to a large-scale magnetosheath plasma jet: THEMIS and ground-based observations. *Journal of Geophysical Research: Space Physics*, *117*(8), 1–16. doi: 10.1029/2011JA016861

Dmitriev, A. V., & Suvorova, A. V. (2015). Large-scale jets in the magnetosheath and plasma penetration across the magnetopause: Themis observations. *Journal of Geophysical Research: Space Physics*, *120*(6), 4423-4437. doi: 10.1002/2014JA020953

Ebert, R. W., McComas, D. J., Elliott, H. A., Forsyth, R. J., & Gosling, J. T. (2009). Bulk properties of the slow and fast solar wind and interplanetary coronal mass ejections measured by Ulysses: Three polar orbits of observations. *Journal of Geophysical Research: Space Physics*, *114*(1). doi: 10.1029/2008JA013631

Goncharov, O., Gunell, H., Hamrin, M., & Chong, S. (2020). Evolution of High-Speed Jets and Plasmoids Downstream of the Quasi-Perpendicular Bow Shock. *Journal of Geophysical Research: Space Physics*, *125*(6), 1–16. doi: 10.1029/2019JA027667

Hietala, H., Laitinen, T. V., Andréeová, K., Vainio, R., Vaivads, A., Palmroth, M., ... Rème, H. (2009). Supermagnetosonic jets behind a collisionless quasiparallel shock. *Physical Review Letters*, *103*(24), 20–23. doi: 10.1103/PhysRevLett.103.245001

Hietala, H., Partamies, N., Laitinen, T. V., Clausen, L. B., Facskò, G., Vaivads, A., ... Lucek, E. A. (2012). Supermagnetosonic subsolar magnetosheath jets and their effects: From the solar wind to the ionospheric convection. *Annales Geophysicae*, *30*(1), 33–48. doi: 10.5194/angeo-30-33-2012

Hietala, H., Phan, T. D., Angelopoulos, V., Oieroset, M., Archer, M. O., Karlsson, T., & Plaschke, F. (2018). In Situ Observations of a Magnetosheath High-Speed Jet Triggering Magnetopause Reconnection. *Geophysical Research Letters*, *45*(4), 1732–1740. doi: 10.1002/2017GL076525

Jian, L., Russell, C. T., Luhmann, J. G., & Skoug, R. M. (2006). Properties of Stream Interactions at One AU During 1995 – 2004. *Solar Physics*, *239*(1), 337–392. doi: 10.1007/s11207-006-0132-3

Karimabadi, H., Roytershteyn, V., Vu, H. X., Omelchenko, Y. A., Scudder, J., Daughton, W., ... Geveci, B. (2014). The link between shocks, turbulence, and magnetic reconnection in collisionless plasmas. *Physics of Plasmas*, *21*(6). doi: 10.1063/1.4882875

Karlsson, T., Kullen, A., Liljeblad, E., Brenning, N., Nilsson, H., Gunell, H., & Hamrin, M. (2015). On the origin of magnetosheath plasmoids and their relation to magnetosheath jets. *Journal of Geophysical Research A: Space Physics*, *120*(9). doi: 10.1002/2015JA021487

Kilpua, E. K., Balogh, A., von Steiger, R., & Liu, Y. D. (2017). Geoeffective Properties of Solar Transients and Stream Interaction Regions. *Space Science Reviews*, *212*(3-4), 1271–1314. doi: 10.1007/s11214-017-0411-3

King, J. H., & Papitashvili, N. E. (2005). Solar wind spatial scales in and comparisons of hourly Wind and ACE plasma and magnetic field data. *Journal of Geophysical Research: Space Physics*, *110*(A2), 1–9. doi: 10.1029/2004JA010649

Liu, T. Z., Hietala, H., Angelopoulos, V., Omelchenko, Y., Vainio, R., & Plaschke, F. (2020). Statistical Study of Magnetosheath Jet-Driven Bow Waves. *Journal of Geophysical Research: Space Physics*, *125*(7), 1–14. doi: 10.1029/2019JA027710

McComas, D. J., Elliott, H. A., Schwadron, N. A., Gosling, J. T., Skoug, R. M., & Goldstein, B. E. (2003). The three-dimensional solar wind around solar maximum. *Geophysical Research Letters*, *30*(10), 1–4. doi: 10.1029/2003gl017136

Merka, J., Szabo, A., Slavin, J. A., & Peredo, M. (2005). Three-dimensional position and shape of the bow shock and their variation with upstream Mach numbers and interplanetary magnetic field orientation. *Journal of Geophysical Research: Space Physics*, *110*(A4). doi: 10.1029/2004JA010944

Neugebauer, M., Goldstein, R., & Goldstein, B. E. (1997). Features observed in the trailing regions of interplanetary clouds from coronal mass ejections. *Journal of Geophysical Research A: Space Physics*, *102*(A9), 19743–19751. doi: 10.1029/97JA01651

Nykyri, K., Bengtson, M., Angelopoulos, V., Nishimura, Y., & Wing, S. (2019).

Can Enhanced Flux Loading by High-Speed Jets Lead to a Substorm? Multipoint Detection of the Christmas Day Substorm Onset at 08:17 UT, 2015. *Journal of Geophysical Research: Space Physics*, *124*(6), 4314–4340. doi: 10.1029/2018JA026357

Omidi, N., Berchem, J., Sibeck, D., & Zhang, H. (2016). Impacts of spontaneous hot flow anomalies on the magnetosheath and magnetopause. *Journal of Geophysical Research: Space Physics*, *121*(4), 3155-3169. doi: 10.1002/2015JA022170

Palmroth, M., Hietala, H., Plaschke, F., Archer, M., Karlsson, T., Blanco-Cano, X., ... Turc, L. (2018). Magnetosheath jet properties and evolution as determined by a global hybrid-Vlasov simulation. *Annales Geophysicae*, *36*(5), 1171–1182. doi: 10.5194/angeo-36-1171-2018

Palmroth, M., Raptis, S., Suni, J., Karlsson, T., Turc, L., Johlander, A., ... Osmane, A. (2021). Magnetosheath jet evolution as a function of lifetime: global hybrid-vlasov simulations compared to mms observations. *Annales Geophysicae*, *39*(2), 289–308. doi: 10.5194/angeo-39-289-2021

Plaschke, F., Glassmeier, K. H., Sibeck, D. G., Auster, H. U., Constantinescu, O. D., Angelopoulos, V., & Magnes, W. (2009). Magnetopause surface oscillation frequencies at different solar wind conditions. *Annales Geophysicae*, *27*(12), 4521–4532. doi: 10.5194/angeo-27-4521-2009

Plaschke, F., Hietala, H., & Angelopoulos, V. (2013). Anti-sunward high-speed jets in the subsolar magnetosheath. *Annales Geophysicae*, *31*(10), 1877–1889. doi: 10.5194/angeo-31-1877-2013

Plaschke, F., Hietala, H., & Angelopoulos, V. (2020, Aug). *Anti-sunward high-speed jets in the subsolar magnetosheath: Data sets.* OSF. Retrieved from `osf.io/gf732`

Plaschke, F., Hietala, H., Angelopoulos, V., & Nakamura, R. (2016). Geoeffective jets impacting the magnetopause. *Journal of Geophysical Research: Space Physics*. doi: 10.1002/2016JA022534

Plaschke, F., Hietala, H., Archer, M., Blanco-Cano, X., Kajdič, P., Karlsson, T., ... Sibeck, D. (2018). Jets Downstream of Collisionless Shocks. *Space Science Reviews*, *214*(5). doi: 10.1007/s11214-018-0516-3

Plaschke, F., Hietala, H., & LaMoury, A. T. (2020, Oct). *THEMIS magnetosheath jet data set 2012-2018.* OSF. Retrieved from `osf.io/7rjs4`

Plaschke, F., Hietala, H., & Vörös, Z. (2020). Scale Sizes of Magnetosheath Jets. *Journal of Geophysical Research: Space Physics*, *125*(9). doi: 10.1029/2020JA027962

Raptis, S., Karlsson, T., Plaschke, F., Kullen, A., & Lindqvist, P. A. (2020). Classifying Magnetosheath Jets Using MMS: Statistical Properties. *Journal of Geophysical Research: Space Physics*, *125*(11). doi: 10.1029/2019JA027754

Schwartz, S. J., & Burgess, D. (1991). Quasi-parallel shocks: A patchwork of three-dimensional structures. *Geophysical Research Letters*, *18*(3), 373–376. doi: 10.1029/91GL00138

Shue, J.-H., Chao, J. K., Song, P., McFadden, J. P., Suvorova, A., Angelopoulos, V., ... Plaschke, F. (2009). Anomalous magnetosheath flows and distorted subsolar magnetopause for radial interplanetary magnetic fields. *Geophysical Research Letters*, *36*(18), 3–7. doi: 10.1029/2009GL039842

Shue, J.-H., Song, P., Russell, C. T., Steinberg, J. T., Chao, J. K., Zastenker, G., ... Kawano, H. (1998). Magnetopause location under extreme solar wind conditions. *Journal of Geophysical Research: Space Physics*, *103*(A8), 17691–17700. doi: 10.1029/98ja01103

Suvorova, A. V., Shue, J. H., Dmitriev, A. V., Sibeck, D. G., McFadden, J. P., Hasegawa, H., ... Němeček, Z. (2010). Magnetopause expansions for quasi-radial interplanetary magnetic field: THEMIS and Geotail observations. *Journal of Geophysical Research: Space Physics*, *115*(10), 1–16. doi: 10.1029/2010JA015404

Swisdak, M., Opher, M., Drake, J. F., & Alouani Bibi, F. (2010). The vector direction of the interstellar magnetic field outside the heliosphere. *Astrophysical Journal*, *710*(2), 1769–1775. doi: 10.1088/0004-637X/710/2/1769

Turc, L., Ganse, U., Pfau-Kempf, Y., Hoilijoki, S., Battarbee, M., Juusola, L., ... Palmroth, M. (2018). Foreshock Properties at Typical and Enhanced Interplanetary Magnetic Field Strengths: Results From Hybrid-Vlasov Simulations. *Journal of Geophysical Research: Space Physics*, *123*(7), 5476–5493. doi: 10.1029/2018JA025466

Turc, L., Roberts, O. W., Archer, M. O., Palmroth, M., Battarbee, M., Brito, T., ... Dandouras, I. (2019). First Observations of the Disruption of the Earth's Foreshock Wave Field During Magnetic Clouds. *Geophysical Research Letters*, *46*(22), 12644–12653. doi: 10.1029/2019GL084437

Vuorinen, L., Hietala, H., & Plaschke, F. (2019). Jets in the magnetosheath: IMF control of where they occur. *Annales Geophysicae*, *37*(4), 689–697. doi: 10.5194/angeo-37-689-2019

Wang, B., Nishimura, Y., Hietala, H., Lyons, L., Angelopoulos, V., Plaschke, F., ... Weatherwax, A. (2018). Impacts of Magnetosheath High-Speed Jets on the Magnetosphere and Ionosphere Measured by Optical Imaging and Satellite Observations. *Journal of Geophysical Research: Space Physics*, *123*(6), 4879–4894. doi: 10.1029/2017JA024954